



# Seismotectonic significance of the December 1, 2020 Haridwar, India earthquake ( $M$ 4.3), a lower crust event near the Himalayan topographic front

T C SUNILKUMAR<sup>1,\*</sup> , VINEET K GAHALAUT<sup>1</sup>, D SRINAGESH<sup>1,2</sup> and B NARESH<sup>1</sup>

<sup>1</sup>*CSIR-National Geophysical Research Institute, Uppal Road, Hyderabad 500 007, India.*

<sup>2</sup>*Department of Civil Engineering, Indian Institute of Technology Madras, Chennai 600 036, India.*

\*Corresponding author. e-mail: tcsunilkumartc@gmail.com

MS received 8 November 2021; revised 19 August 2022; accepted 17 December 2022

Earthquakes in the Himalayan arc occur due to the interaction of Indian and Eurasian plates, and a great majority of them are of interplate type, occurring on the Main Himalayan Thrust (MHT). Some earthquakes, however, occur south of the Himalayan arc within the subducting Indian plate and majority of these earthquakes occur on the subducting ridges of the Indian plate, the most prominent of which is the Delhi–Haridwar ridge. The December 1, 2020 ( $M_L$  4.3,  $M_W$  3.8) earthquake is one such event whose source parameters are very well constrained by the local network installed in the region. The earthquake occurred close to the Himalayan Frontal Thrust at a depth of 36 km. The estimated focal mechanism from moment tensor inversion shows a strike-slip mechanism, with P-axis orientation concurrent with Indian plate motion with respect to Eurasia. The stress drop of  $9.4 \pm 3.7$  MPa is consistent with relatively higher stress drop in intraplate earthquakes. Based on the estimated parameters, we qualitatively evaluated whether it occurred (i) on the newly discovered southernmost deformation front, referred as the piedmont fault, which developed in response to the southward propagation of the Himalayan wedge, (ii) due to flexure in the Indian plate caused by long term subduction, (iii) due to strong coupling on the MHT causing flexure in the foreland, and (iv) on the northward extension of the Delhi Haridwar ridge. We propose that it probably occurred on the northward continuation of the Delhi–Haridwar ridge as similar earthquakes occur on this ridge in and around the Delhi region. We also suggest that the 1988 Udaipur (Nepal) earthquake, which had a similar focal depth, location, and focal mechanism, occurred on the Munger–Saharsa ridge’s northward continuation. The strong coupling on the MHT in the adjoining Himalayan segments might have helped in the occurrence of both earthquakes.

**Keywords.** Earthquakes; Delhi–Haridwar ridge; Himalayan arc; focal mechanism.

## 1. Introduction

Himalayan arc is one of the most seismically active convergent boundaries, having potential to generate large earthquakes due to the ongoing

continental–continental collision between the Indian and Eurasian plates (figure 1). The earthquakes that have caused the most damage in the last two centuries in the Himalayan and contiguous plains are: 1803 Garhwal ( $M_W$  7.6), 1897 Assam



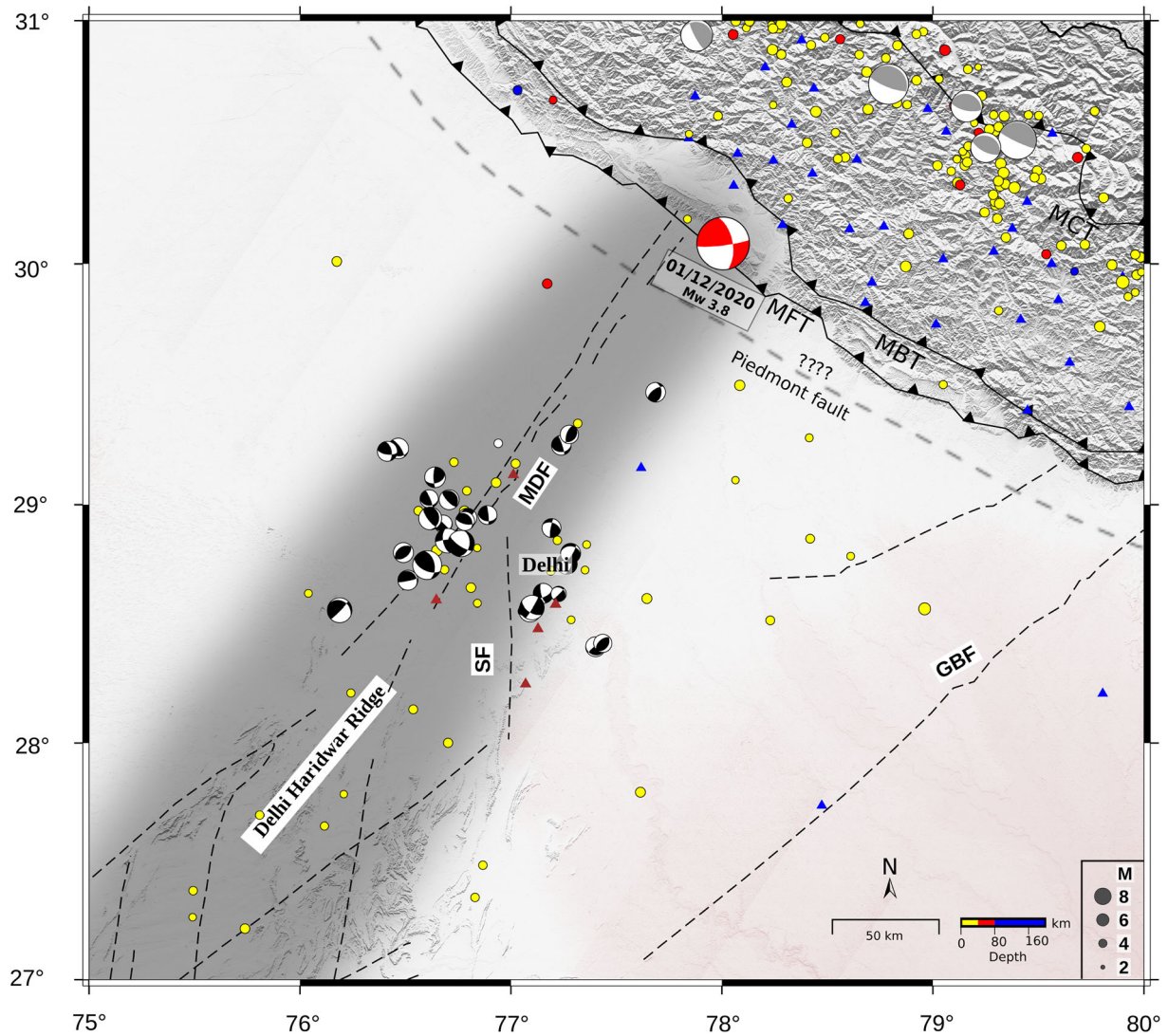


Figure 2. Seismotectonic map of the study area. Significant events (1900–2021, NEIC) from this region are plotted. The focal mechanism of December 1, 2020 (from fociMT) with compressional quadrant shaded in red colour (not scaled with magnitude) is shown and is showing strike-slip mechanism with NNE P-axis. Focal mechanisms with black-coloured compressional quadrant represent the event nearby Delhi–Haridwar ridge from the various study. Focal mechanisms with grey compressional quadrant (1976–2021, GCMT) represent events along the Himalayan arc. Blue triangle represents the local seismic network around the source region operated by CSIR-NGRI. Brown colour triangles denote NCS stations. Major seismotectonic features are shown as SF: Sohna Fault; GBF: Great Boundary Fault; MDF: Mahendragarh–Dehradun Fault. Approximate location of piedmont fault is after Yeats and Thakur (2008).

sediments beneath the Gangetic plain range from 1 to 6 km (Lyon-Caen and Molnar 1985; Borah *et al.* 2015). At least three aseismic ridges, namely, Aravalli–Delhi fold belt (ADFB), Faizabad ridge and Munger–Saharsa ridge on the Indian plate extend beneath the Indo-Gangetic plains and possibly extend northward beneath the Himalayan wedge. The ADFB is the most prominent amongst them and includes several mapped/inferred faults, e.g., the Great Boundary Fault (GBF), Sohna Fault, Delhi–Haridwar Ridge, Mathura Fault, and Moradabad Fault (Valdiya 1976; Dasgupta *et al.*

1987). Most earthquakes of the ADFB show reverse or oblique motion on steep dipping faults (Shukla *et al.* 2007). The northward extension of ADFB beneath the Indo-Gangetic plains appears to be less seismogenic as compared to its southward extension. The 2020 Haridwar earthquake is apparently located on the northward extension of the ADFB. Despite its smaller magnitude ( $M$  4.3), it is critical to understand its source mechanism, occurrence process and its tectonic implications on the Himalayan and foreland seismo-tectonic systems for future hazard assessment.



## 2. Data

CSIR-NGRI is operating a local network in the Uttarakhand and adjoining Indo-Gangetic plains with broadband sensors (figure 2). A total of 45 broadband and five strong motion seismic stations data along with five stations operated by the National Center for Seismology (phase data available at ISC) were used for locating the earthquake by using SEISAN software (ver. 11) (Ottemöller *et al.* 2013). The nearest and farthest stations used here are located at 45 and 270 km, respectively. The estimated hypocentre location is at 30.057°N and 77.964°E with a depth of 36 km (35.8 km) with an uncertainty of <2 km corresponding to an RMS error in travel time of 0.3 s. The magnitude of the earthquake  $M_L$  is 4.3. Inclusion of NCS stations helped in adequately covering the hypocentre with no azimuthal gap (figure 2).

## 3. Source characteristics

### 3.1 Focal mechanism

Over a wide range of magnitudes, the seismic moment tensor has been used as a standard parameter for understanding earthquake kinematics source processes. Globally, for larger earthquakes ( $M_W > 4.5$ ), source parameters are routinely done using teleseismic waveforms by the Harvard Centroid Moment Tensor (CMT) project (e.g., Ekström *et al.* 2012) and by the United States Geological Service (USGS) (e.g., Sipkin and Needham 1993). For  $M_W \leq 4.5$  earthquakes, moment tensor solutions require local or regional data (e.g., Ford *et al.* 2009; Vavryuk and Kim 2014). The MT inversion may be performed using a variety of input data from body-wave amplitudes to full waveforms.

To determine the focal mechanism of the earthquake, we first used a full waveform inversion algorithm as implemented in the ISOLA program package (Sokos and Zahradnik 2008). ISOLA is widely established as a reliable program for estimating focal mechanisms of varying magnitudes at local and regional distances. ISOLA is based on an extension of the method proposed by Kikuchi and Kanamori (1991) to regional and local distances. One of the most important steps in the analysis is the selection of an appropriate crustal model to compute Green's function which represents the earth's response as it plays an important role in

estimating Green's function. The inversion is performed in the time domain while the Earth response is represented by Green's function computed based on discrete wavenumber algorithm (Bouchon 1981) using 1-D velocity model of Borah *et al.* (2015). During inversion, the seismograms were filtered in the frequency range between 0.13 and 0.18 Hz. The MT inversion is retrieved by the least-squares inversion and the best matching between observed and synthetic waveforms can be shown based on variance reduction values (VR) (Sokos and Zahradnik 2008). The best fit double couple model has a VR value of 0.57 and reveals the mechanism of predominantly strike-slip in nature with nodal planes oriented in the ENE–WSW (NP1: strike,  $\phi = 70^\circ$ , dip,  $\delta = 83^\circ$ , rake,  $\lambda = 33^\circ$ ) and NW–SE (NP2:  $\phi = 336^\circ$ ,  $\delta = 57^\circ$ ,  $\lambda = 172^\circ$ ) directions (figure 3). The estimated depth of 36 km is similar to that estimated using phase data (figure 3b). The magnitude is estimated as  $M_W$  3.8.

The focal mechanism is further confirmed using the polarity of first arrivals and P-wave spectra to constrain double-couple MT solution (Kwiatek *et al.* 2016). We use fociMT inversion method which is based on the concept of Fitch *et al.* (1980) and Wiejacz (1992). The input data for the MT inversion are the P-wave spectra and first motion polarities of the vertical components (Kwiatek *et al.* 2016). We selected stations having clear P-arrival around the event and estimated the focal mechanism, which is predominantly strike-slip in nature with nodal planes oriented in the ENE–WSW (NP1: strike,  $\phi = 83^\circ$ , dip,  $\delta = 83^\circ$ , rake,  $\lambda = 30^\circ$ ) and NW–SE (NP2:  $\phi = 349^\circ$ ,  $\delta = 60^\circ$ ,  $\lambda = 172^\circ$ ) directions and the P-axis is oriented in the NNE direction (figure 2) which is similar to that obtained using the waveform inversion. The estimated  $M_W$  is 3.9.

### 3.2 Source parameters

The frequency analysis method is more commonly used for estimating basic source parameters (e.g., Abercrombie and Rice 2005; Mandal and Johnston 2006; Allmann and Shearer 2007) using Brune's (1970, 1971) theoretical spectrum of circular rupture model for small earthquakes, which includes a flat plateau at low frequencies and decreases by  $\omega^{-2}$  at high frequencies. Using the SourceSpec Python package (Satriano 2020), we determined the source parameter using S-wave spectra. The combined

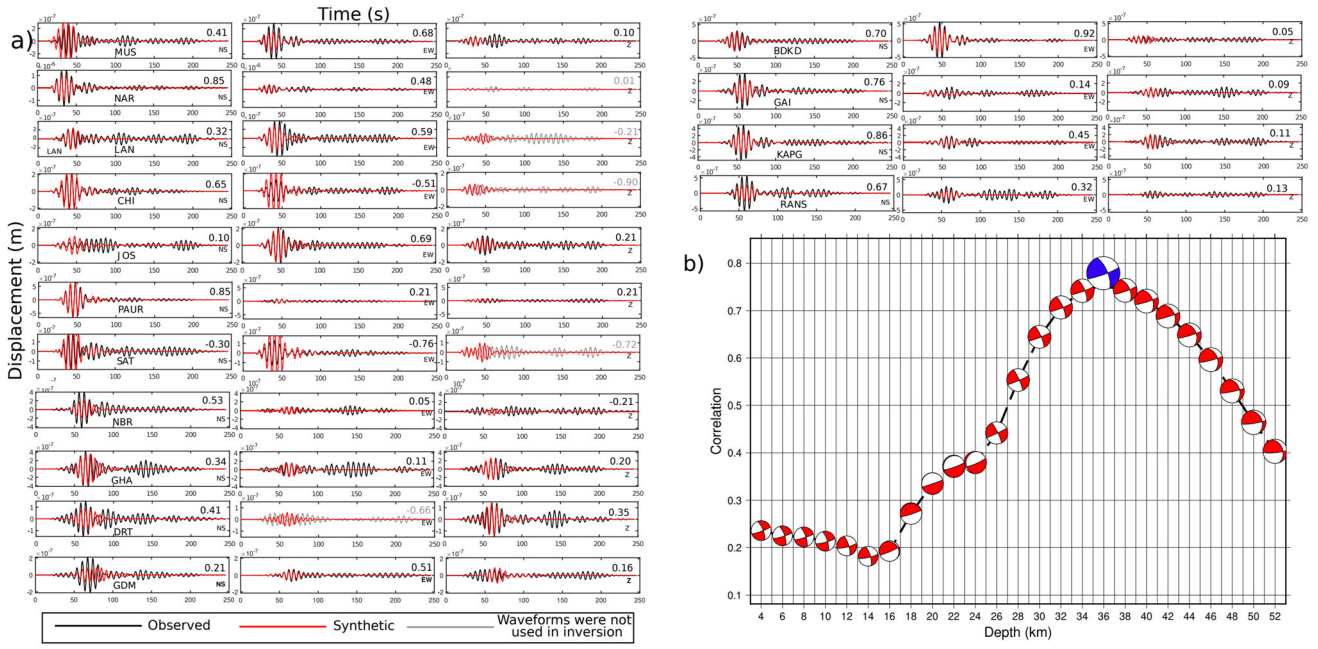


Figure 3. Moment tensor inversion result for the 1 December 2021, Haridwar earthquake. (a) Comparison of observed (black) and synthetic (red) waveforms. Station name in each case is indicated in the N-S component. The number at the right top in the waveform panel represents the variance reduction between the waveforms. (b) The best-fitting mechanism for different trial depths is plotted in a lower hemisphere projection. The best fit is for a depth of 36 km (blue colour).

effect of the source, crustal wave propagation, and site contributions determine the amplitude spectrum of ground motion for a given distance  $R$  from the earthquake source, as shown below:

$$v(f, R) = \Omega_0(f) \cdot 2\pi f \cdot A(f, R) \cdot H(f) \quad (1)$$

where  $v(f, R)$  is the velocity and  $f$  is the frequency,  $A(f, R)$  is seismic wave attenuation factor along the source-to-station propagation path, and  $H(f)$  is a site term accounting for near-surface propagation effects beneath the station.

The source-radiated displacement spectrum is expressed as:

$$\Omega_0(f) = \frac{F_s R_{\theta, \varphi}}{4\pi \rho R \beta^3} \cdot \frac{M_0}{1 + (f/f_c)^2} \quad (2)$$

Here  $M_0$  and  $f_c$  are seismic moment and corner frequency, respectively.  $R_{\theta, \varphi}$  is the radiation pattern, which represents the average  $S$  wave radiation pattern over azimuth and take-off angles and is taken equal to 0.55 (Boore and Boatwright 1984).  $R$  is the hypocentral distance.  $F_s$  accounts for the free-surface effect, taken equal to 2.  $\rho$  and  $\beta$  are density and shear wave velocity at the source region, respectively.

Following Eshelby (1957), the radius  $r$  and uniform stress drop ( $\Delta\sigma$ ) of a circular crack in an infinite Poisson solid are linked to  $M_0$  and  $f_c$  through the equations:

$$\Delta\sigma = \frac{7}{16} \frac{M_0}{r^3} \quad (3)$$

$$r = \frac{2.34\beta}{2\pi f_c} \quad (4)$$

As far as apparent stress ( $\tau_a$ ) is concerned, we followed the standard method of Wyss and Brune (1968) using the definition

$$\tau_a = \mu \frac{E_r}{M_0} \quad (5)$$

where  $E_r$  is the radiated energy, which is determined following the approach described in Boatwright *et al.* (2002) and Lancieri *et al.* (2012).

The source amplitude spectra of the 2020 event are shown in figure 4, where we used six stations with a good signal-to-noise ratio ( $S/N > 3$ ). The estimated seismic moment ( $M_0$ ) is  $4.9 \times 10^{14}$  Nm, corresponding to an  $M_W$  of  $3.73 (\pm 0.07)$  and a corner frequency ( $f_c$ ) of  $5.1 (\pm 0.6)$ . The fracture

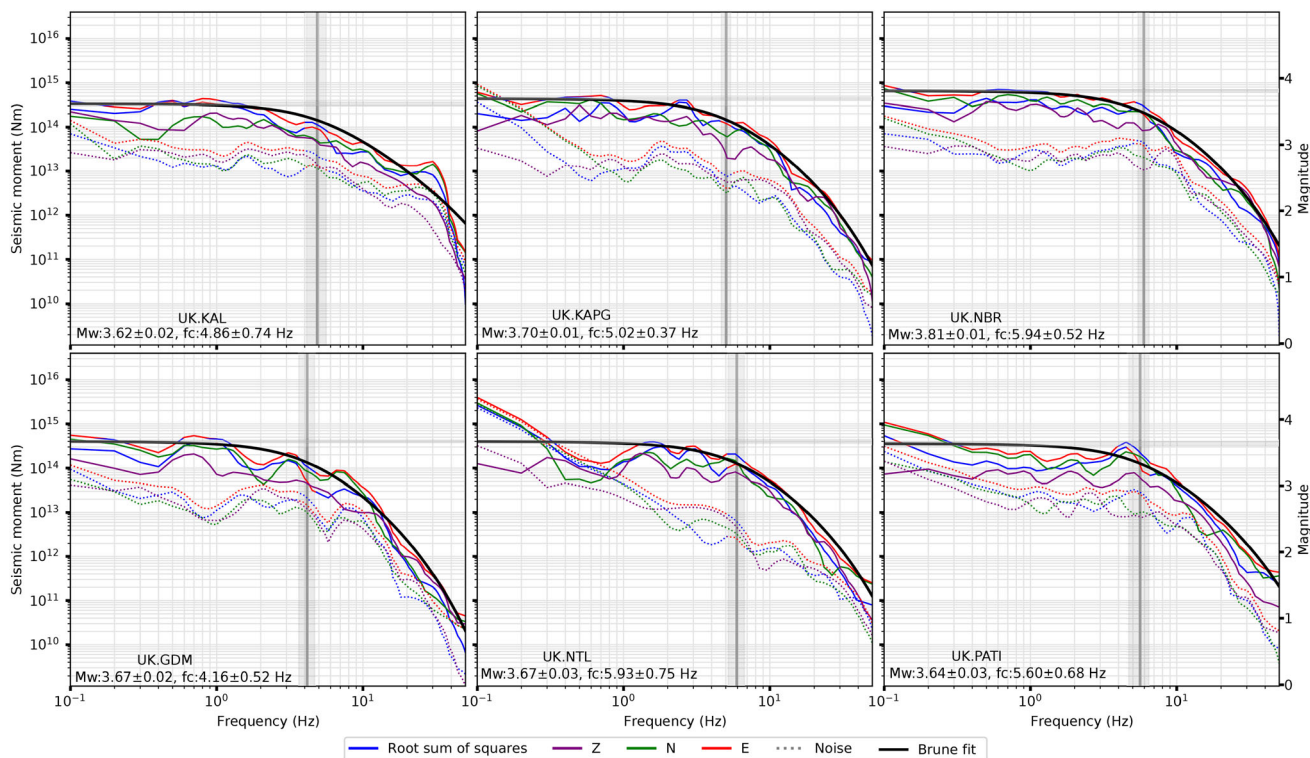


Figure 4. Best fitting of Brune's displacement spectra obtained to estimate source parameters. Estimated average  $M_0$  is  $4.9 \times 10^{14}$  Nm which is equivalent to the  $M_W$  of 3.73 ( $\pm 0.07$ ) and a corner frequency of 5.1 ( $\pm 0.6$ ).

radius is approximately 269 ( $\pm 32$ ) m. A value of  $9.4 \pm 3.7$  MPa and  $3.03 \times 10^{10}$  J are obtained for the stress drop ( $\Delta\sigma$ ) and estimated radiated energy ( $E_r$ ), respectively. The scaled energy which is the ratio of radiated energy and  $M_0$  is  $6.2 \times 10^{-5}$ . The calculated apparent stress drop ( $\tau_a$ ) is 2.5 MPa based on the assumption of a rigidity modulus ( $\mu$ ) of  $4.03 \times 10^{10}$  Pa from the velocity model of Borah *et al.* (2015) at the source depth of the event.

#### 4. Discussion

The occurrence of an event like December 2020 at a depth of 36 km within the Indian plate and  $\sim 20$  km south of the mountain front, is rare. It is an intraplate earthquake which occurred on the Delhi–Haridwar ridge beneath the 5–6 km thick sediments of Indo-Gangetic plains. Data from our dense and close seismic network, along with the data from NCS stations, provided us the opportunity to look into the source characteristics of the 2020 Haridwar event to understand the causative reason and its seismotectonic implications. The estimated focal mechanism suggests that predominant sinistral or dextral strike-slip motion was

involved on the ENE–WSW or NW–SE oriented nodal plane, respectively, which is consistent with the stress regime inferred from the earthquakes in the Delhi region (figures 2 and 3). The earthquake's depth is comparable with earthquakes in the Delhi region, which occur at depths of up to 30 km (figure 5). The estimated stress drop of 9.4 MPa for the event implies high-stress drop and is consistent with the higher stress drop for the stable continental events. Lower strain rates and longer average fault healing time in the intraplate zone (Scholz 2002; Venkataraman and Kanamori 2004) could explain the larger stress drop and probably related to the strike-slip mechanism of the events (Allmann and Shearer 2007). It was observed that there is no relation between stress drop and magnitude (Venkataraman and Kanamori 2004; Allmann and Shearer 2007). Previous research by Sharma and Wason (1994) and Sivaram *et al.* (2013) found that the stress drop estimated for the interplate earthquake from the Kumaun Himalayan region is  $< 1$  MPa for similar magnitude events. In fact, large value of stress drop of 13 MPa for November 25, 2007 ( $M_W$  4.1) (Singh *et al.* 2010) and 12.4 MPa for March 5, 2012 ( $M_W$  4.6) (Mittal *et al.* 2016) earthquakes in the Delhi region has

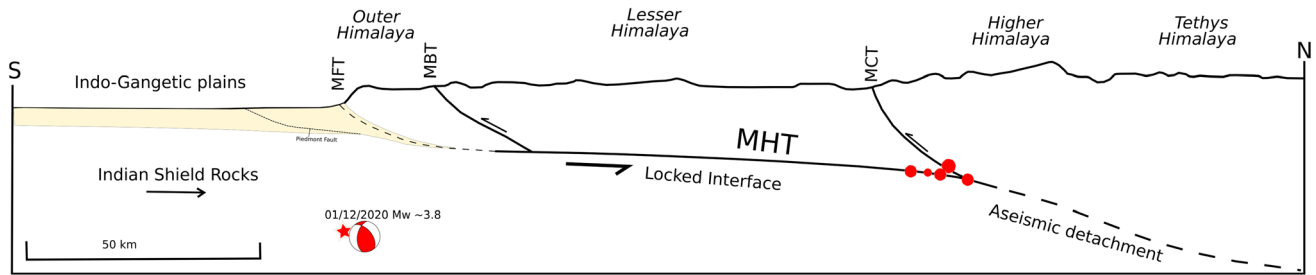


Figure 5. General depth section of Himalaya. Based on the depth estimation, the epicentre location of December 1, 2020 Haridwar events is marked with focal mechanism and indicates intraplate origin. MFT, MBT, MCT, and MHT are also marked.

been reported. Further, similar high-stress drop estimates have been reported for other significant intraplate earthquakes in India, e.g., 21 MPa for the 2001 Bhuj mainshock of  $M_W$  7.7 (Negishi *et al.* 2001; Antolik and Dreger 2001), 7 MPa for the 1993 Latur earthquake of  $M_W$  6.3 (Baumbach *et al.* 1994) and about 20 MPa for the  $M_W$  5.8 Jabalpur earthquake (Singh *et al.* 1999). The scaled energy, expressed as a ratio of  $E_r$  to  $M_0$  is an order of  $10^{-5}$ . In general, the ratio of energy to moment is  $10^{-6}$ – $10^{-5}$  for smaller events, but for the larger events ( $>10^{16}$  Nm), the ratio increases to between  $10^{-5}$  and  $10^{-4}$  (Venkataraman and Kanamori 2004). Our estimated value of  $6.2 \times 10^{-5}$  is higher than the average for this type of magnitude which could be due to the higher stress drop and fault strength.

Farther south of the Haridwar event along the ADFB, near Delhi, many moderate and smaller magnitude earthquakes have occurred. Although the overall trend of ADFB is NE–SW, there are several faults within ADFB which criss-cross ADFB. It is difficult to associate these earthquakes to an identified fault in the region. Their focal mechanisms generally exhibit oblique (strike-slip and reverse motion on steep faults) motion on the faults which are generally transverse to the trend of ADFB. The 2020 Haridwar earthquake is quite similar to the earthquakes of Delhi region in terms of focal mechanism and sense of motion.

One of the critical questions here is the seismogenesis of this earthquake. We qualitatively evaluated all possibilities for the 2020 Haridwar earthquake occurrence based on the estimated source parameters. We examined the possibilities of whether this earthquake occurred (i) in response to the southward propagation of the Himalayan wedge in the form of piedmont fault, (ii) due to

flexure in the Indian plate caused by the subduction of the Indian plate beneath Eurasia along the Himalayan arc, (iii) due to strong coupling on the MHT, and (iv) on the northward extension of the Delhi–Haridwar ridge. The first hypothesis can be refuted straight away, and as it occurred at 36 km depth we confirm that the earthquake did not happen on the piedmont fault. In the Indo-Gangetic plains of Pakistan and India, Yeats and Thakur (2008) proposed a southerly progression of thrust front and identified piedmont fault. In the region of earthquake, they mapped piedmont fault at about 20 km south of the Main Frontal Thrust (MFT), the southernmost thrust fault or the deformation front of the Himalayan arc. Although the epicentre of the earthquake is closer to the MFT ( $\sim 3$ – $4$  km south of the MFT), it is unrelated to any of these surface-mapped faults in the Himalayan wedge or on the Indo-Gangetic plains due to its deeper focal depth. Even the second and third hypotheses, i.e., the flexure on the Indian plate due to Indian plate subduction, also caused by the strong locking on the MHT, similar to the subduction zone’s outer rise earthquakes (e.g., Chapple and Forsyth 1979; Christensen and Ruff 1988; Craig *et al.* 2014), can be refuted due to larger focal depth of this earthquake. The outer rise earthquakes are generally shallow and involve normal faulting, which is not the case for the 2020 Haridwar earthquake. We propose that it probably occurred on the northward continuation of the Delhi–Haridwar ridge as similar earthquakes occur on this ridge in and around Delhi region. Similar to the Haridwar earthquake, a strong earthquake in 1988 Udaipur (Nepal) with a magnitude of 6.8, occurred on the northward extension of the Munger–Saharsa ridge, with similar focal depth, location, and focal mechanism (Chen and Kao 1996;



Ghimire and Kasahara 2007). However, the Munger–Saharsa ridge is not as active as the ADFB, but that could be due to lack of nearby seismic stations close to Munger–Saharsa ridge. In fact, the occurrence of 1988 and 2020 type of earthquakes pose an additional seismic hazard. So far our perception of hazards in the Himalaya and adjoining regions is limited to that posed by the Himalayan earthquakes on the MHT. But the occurrence of these earthquakes, though at relatively deeper depths, may pose additional hazards if the magnitude of such earthquake is large, as witnessed during the 1988 earthquake of  $M_W$  6.8, which took  $\sim 1000$  lives.

## 5. Conclusions

The 2020 Haridwar earthquake is unusual in terms of its location, focal depth and source parameters. We estimated its source parameters using a dense and local seismic network around it. The earthquake occurred at 36 km within the Indian plate and south of Himalayan convergent boundary. It involved strike-slip motion on steep planes and exhibited relatively higher stress drop. It appears to have occurred on the northward extension of Aravalli–Delhi fold belt, which in this part is buried under the 5–6 km thick Indo-Gangetic plains. The source parameters of this earthquake are also similar to that of the earthquakes in the Aravalli–Delhi fold belt. We recall that a similar but of larger magnitude earthquake ( $M_W$  6.8 1988 Udairpur, Nepal earthquake) occurred on the northward extension of Munger–Saharsa ridge. Occurrence of such earthquakes on the ridges on the Indian plate, which are extending northward and subduction beneath the Himalayan wedge, pose additional seismic hazard which is generally not considered as we tend to focus on the seismic hazard posed by the Himalayan earthquakes occurring on the MHT. We acknowledge that although they are rare events, they can still pose significant seismic hazards.

## Acknowledgements

We are thankful to the Director, CSIR-NGRI, Hyderabad, for his support and permission to publish this work. Maps were plotted using Generic Mapping Tools (Wessel and Smith 1998). NCS station phase data were used from ISC website. We

thank the Editor and anonymous reviewers for their constructive comments.

## Authors statement

T C Sunilkumar: Conception, estimation of focal mechanism and source parameters; V K Gahalaut: Conception, manuscript preparation and supervision; Naresh Bandari: Data collection and estimation of earthquake parameters; D Srinagesh: Took initiative in deploying the network. All the authors contributed equally in writing the manuscript.

## References

- Abercrombie R E and Rice J R 2005 Can observations of earthquake scaling constrain slip weakening?; *Geophys. J. Int.* **162**(2) 406–424.
- Allmann B P and Shearer P M 2007 Spatial and temporal stress drop variations in small earthquakes near Parkfield, California; *J. Geophys. Res.: Solid Earth* **112**(B4).
- Altamimi Z, Métivier L and Collilieux X 2012 ITRF2008 plate motion model; *J. Geophys. Res.: Solid Earth* **117**(B7).
- Antolik M and Dreger D 2001 Source rupture process of the 26 January, 2001 Bhuj, India, earthquake (M 7.6); AGU Fall Meeting Abstracts, Vol. 2001, pp. S52G-03.
- Baumbach M, Grosser H, Schmidt H, Paulat A, Rietbrock A, Rao C R, Raju P S, Sarkar D and Mohan I 1994 Study of foreshocks and aftershocks of the intraplate Latur earthquake of September 30, 1993, India; *Geol. Soc. India Memoir* **35** 33–63.
- Bilham R, Gaur V K and Molnar P 2001 Himalayan seismic hazard; *Science* **293**(5534) 1442–1444.
- Boatwright J, Choy G L and Seekins L C 2002 Regional estimates of radiated seismic energy; *Bull. Seismol. Soc. Am.* **92**(4) 1241–1255.
- Boore D M and Boatwright J 1984 Average body-wave radiation coefficients; *Bull. Seismol. Soc. Am.* **74**(5) 1615–1621.
- Borah K, Kanna N, Rai S and Prakasam K 2015 Sediment thickness beneath the Indo-Gangetic plain and Siwalik Himalaya inferred from receiver function modelling; *J. Asian Earth Sci.* **99** 41–56.
- Bouchon M 1981 A simple method to calculate Green's functions for elastic layered media; *Bull. Seismol. Soc. Am.* **71**(4) 959–971.
- Brune J N 1970 Tectonic stress and the spectra of seismic shear waves from earthquakes; *J. Geophys. Res.* **75**(26) 4997–5009.
- Brune J N 1971 Correction to tectonic stress and the spectra of seismic shear waves from earthquakes; *J. Geophys. Res.* **76**(20) 5002.
- Cattin R and Avouac J 2000 Modeling mountain building and the seismic cycle in the Himalaya of Nepal; *J. Geophys. Res.: Solid Earth* **105**(B6) 13,389–13,407.



- Chapple W M and Forsyth D W 1979 Earthquakes and bending of plates at trenches; *J. Geophys. Res.: Solid Earth* **84**(B12) 6729–6749.
- Chen W-P and Kao H 1996 Seismotectonics of Asia: Some recent progress; In: *The Tectonic Evolution of Asia* (eds) Yin A and Harrison M, Cambridge University Press, Cambridge, UK, pp. 37–62.
- Christensen D H and Ruff L J 1988 Seismic coupling and outer rise earthquakes; *J. Geophys. Res.: Solid Earth* **93**(B11) 13,421–13,444.
- Craig T, Copley A and Jackson J 2014 A reassessment of outer-rise seismicity and its implications for the mechanics of oceanic lithosphere; *Geophys. J. Int.* **197**(1) 63–89.
- Dasgupta S, Mukhopadhyay M and Nandy D 1987 Active transverse features in the central portion of the Himalaya; *Tectonophysics*. **136**(3–4) 255–264.
- Diehl T, Singer J, Hetényi G, Grujic D, Clinton J, Giardini D, Kissling E and GANSSER Working Group 2017 Seismotectonics of Bhutan: Evidence for segmentation of the Eastern Himalayas and link to foreland deformation; *Earth Planet. Sci. Lett.* **471** 54–64.
- Ekström G, Nettles M and Dziewoński A M 2012 The global CMT project 2004–2010: Centroid-moment tensors for 13,017 earthquakes; *Phys. Earth Planet. Int.* **200** 1–9.
- Eshelby J D 1957 The determination of the elastic field of an ellipsoidal inclusion, and related problems; *Proc. Roy. Soc. Lond. Ser., Math. Phys. Sci.* **241**(1226) 376–396.
- Fitch T J, McCowan D W and Shields M W 1980 Estimation of the seismic moment tensor from teleseismic body wave data with applications to intraplate and mantle earthquakes; *J. Geophys. Res.: Solid Earth* **85**(B7) 3817–3828.
- Ford S R, Dreger D S and Walter W R 2009 Identifying isotropic events using a regional moment tensor inversion; *J. Geophys. Res.: Solid Earth* **114**(B1).
- Ghimire S and Kasahara M 2007 Source process of the Ms 6.6, Udayapur earthquake of Nepal–India border and its tectonic implication; *J. Asian Earth Sci.* **31**(2) 128–138.
- Kikuchi M and Kanamori H 1991 Inversion of complex body waves-III; *Bull. Seismol. Soc. Am.* **81**(6) 2335–2350.
- Kwiatk G, Martínez-Garzón P and Bohnhoff M 2016 HybridMT: A MATLAB/shell environment package for seismic moment tensor inversion and refinement; *Seismol. Res. Lett.* **87**(4) 964–976.
- Lancieri M, Madariaga R and Bonilla F 2012 Spectral scaling of the aftershocks of the Tocopilla 2007 earthquake in northern Chile; *Geophys. J. Int.* **189**(1) 469–480.
- Lavé J and Avouac J P 2000 Active folding of fluvial terraces across the Siwaliks Hills, Himalayas of central Nepal; *J. Geophys. Res.: Solid Earth* **105**(B3) 5735–5770.
- Lyon-Caen H and Molnar P 1985 Gravity anomalies, flexure of the Indian plate, and the structure, support and evolution of the Himalaya and Ganga basin; *Tectonics* **4**(6) 513–538.
- Mandal P and Johnston A 2006 Estimation of source parameters for the aftershocks of the 2001 Mw 7.7 Bhuj earthquake, India; *Pure Appl. Geophys.* **163**(8) 1537–1560.
- Masse R P and Needham R E 1989 NEIC – The national earthquake information center; *Earthq. Volcanoes (USGS)* **21**(1) 4–44.
- Mittal H, Wu Y M, Chen D Y and Chao W A 2016 Stochastic finite modeling of ground motion for March 5, 2012, Mw 4.6 earthquake and scenario greater magnitude earthquake in the proximity of Delhi; *Nat. Hazards* **82**(2) 1123–1146.
- Negishi H, Mori J, Sato H, Singh R and Kumar S 2001 Aftershocks and slip distribution of mainshock, a comprehensive survey of the 26 January 2001 earthquake (Mw 7.7) in the state of Gujarat; Tech. Rep., India. Research Report on Natural Disasters.
- Ottmöller L, Voss P and Havskov J 2013 SEISAN: The earthquake analysis software for Windows, SOLARIS, LINUX and MACKINTOSH Version 9.3, Manual.
- Pandey M, Tandukar R, Avouac J, Lave J and Massot J 1995 Interseismic strain accumulation on the Himalayan crustal ramp (Nepal); *Geophys. Res. Lett.* **22**(7) 751–754.
- Rao M R 1973 The subsurface geology of the Indo-Gangetic plains; *J. Geol. Soc. India* **14**(3) 217–242.
- Sastri V V, Bhandari L L, Raju A T R and Datta A K 1971 Tectonic framework and subsurface stratigraphy of the Ganga basin; *Geol. Soc. India* **12**(3) 222–233.
- Satriano C 2020 SourceSpec–Earthquake source parameters from S-wave displacement spectra, Version 0.9, Zenodo, <https://doi.org/10.5281/zenodo.3765327>.
- Scholz C 2002 *The mechanics of earthquakes and faulting*; Cambridge University Press, Cambridge, 471p.
- Sharma M and Wason H 1994 Occurrence of low stress drop earthquakes in the Garhwal Himalaya region; *Phys. Earth Planet. Int.* **85**(3–4) 265–272.
- Shukla A, Prakash R, Singh R, Mishra P and Bhatnagar A 2007 Seismotectonic implications of Delhi region through fault plane solutions of some recent earthquakes; *Curr. Sci.* **93**(12) 1848–1853.
- Singh S, Dattatrayam R, Shapiro N, Mandal P, Pacheco J and Midha R 1999 Crustal and upper mantle structure of peninsular India and source parameters of the 21 May 1997, Jabalpur earthquake (Mw 5.8): Results from a new regional broadband network; *Bull. Seismol. Soc. Am.* **89**(6) 1631–1641.
- Singh S, Kumar A, Suresh G, Ordaz M, Pacheco J, Sharma M, Bansal B, Dattatrayam R and Reinoso E 2010 Delhi earthquake of 25 November 2007 (Mw 4.1): Implications for seismic hazard; *Curr. Sci.* **99**(7) 939–947.
- Sipkin S A and Needham R E 1993 Moment-tensor solutions estimated using optimal filter theory: Global seismicity, 1991; *Phys. Earth Planet. Int.* **75**(4) 199–204.
- Sivaram K, Kumar D, Teotia S, Rai S and Prakasam K 2013 Source parameters and scaling relations for small earthquakes in Kumaon Himalaya, India; *J. Seismol.* **17**(2) 579–592.
- Sokos E N and Zahradnik J 2008 ISOLA: A Fortran code and a Matlab GUI to perform multiple-point source inversion of seismic data; *Comput. Geosci.* **34**(8) 967–977.
- Stevens V and Avouac J 2015 Interseismic coupling on the main Himalayan thrust; *Geophys. Res. Lett.* **42**(14) 5828–5837.
- Valdiya K 1976 Himalayan transverse faults and folds and their parallelism with subsurface structures of north Indian plains; *Tectonophysics*. **32**(3–4) 353–386.
- Vavryčuk V and Kim S G 2014 Nonisotropic radiation of the 2013 North Korean nuclear explosion; *Geophys. Res. Lett.* **41**(20) 7048–7056.

- Venkataraman A and Kanamori H 2004 Observational constraints on the fracture energy of subduction zone earthquakes; *J. Geophys. Res.: Solid Earth* **109(B5)**.
- Wiejacz P 1992 Badanie mechanizmów wstrząsów górniczych przy wykorzystaniu tensora momentu sejsmicznego; Institute of Geophysics, Polish Academy of Sciences.
- Wyss M and Brune J N 1968 Seismic moment, stress, and source dimensions for earthquakes in the California-Nevada region; *Geophys. Res. Lett.* **73(14)** 4681–4694.
- Yeats R S and Thakur V 2008 Active faulting south of the Himalayan front: Establishing a new plate boundary; *Tectonophys.* **453(1–4)** 63–73.

Corresponding editor: ANAND JOSHI